Journal of Nanophotonics

SPIEDigitalLibrary.org/jnp

# Controlled alignment of bacterial cells with oscillating optical tweezers

Gideon Carmon
Mario Feingold

SPIE

# Controlled alignment of bacterial cells with oscillating optical tweezers

**Gideon Carmon and Mario Feingold**
Ben Gurion University of the Negev, Department of Physics and The Ilse Katz Center for Nanotechnology, Beer Sheva 84105, Israel
mario@bgu.ac.il

**Abstract.** We used optical tweezers to rotate bacterial cells relative to the optical axis. We rapidly oscillate the optical tweezers along an axis normal to the laser beam, thereby obtaining a linear trap. When the linear trap is longer than a trapped rod-shaped bacterial cell, the cell is aligned along the trap axis. Decreasing the length of the trap, we found that the cell rotates away from the image plane toward the optical axis. In the limit of a nonoscillating trap, the cell aligns along the optical axis. A defocused-edge detection method was devised to measure the orientation of the rotated cell from the corresponding phase-contrast images. Our technique can be used to image three-dimensional sub-cellular structures from different viewpoints and therefore may become a useful tool in fluorescence microscopy.  [DOI: 10.1117/1.3590242]

**Keywords:** optical tweezers; 3D imaging; single cell; *E. coli*.

Paper 11042SSR received Feb. 17, 2011; revised manuscript received Apr. 12, 2011; accepted for publication Apr. 18, 2011; published online May 12, 2011.

## 1 Introduction

Since their introduction in 1986 by Ashkin et al.[1] optical tweezers were used to trap and manipulate particles that ranged between 10 nm to several tens of micrometers. The requirements of the various applications, e.g., to drive micromotors, align micromachined components, or mix in microfluidic devices have led to the development of sophisticated optical tweezer setups that allow both trapping and rotating microparticles.

The first approach to rotating a trapped particle used two independent laser beams.[2,3] While each of the beams grips an extended object at a different spot, moving one beam around the other on a circular path forces the trapped object to follow the rotation. In another setup, linear momentum carried by the laser beam is converted to angular momentum of the trapped object.[4] Trapping a microfabricated particle with asymmetrical geometry, the radiation pressure exerts a torque on the object that rotates via a mechanism resembling that of a windmill. A more advanced approach employs the angular momentum carried by the laser beam to rotate trapped objects. For example, when an absorptive particle is trapped in a Laguerre–Gaussian (LG) helical beam carrying orbital angular momentum, it rotates due to the angular momentum transferred through the absorbed light.[5] Other setups use a circularly polarized LG beam carrying both orbital and spin angular momentum to rotate absorptive particles.[6,7] While these setups have enabled a careful study of the properties of high order laser modes, the rotation rates that could be reached were relatively low. The rotation rates are limited by the amount of absorption allowed before particle overheating and trapping degradation set in. On the other hand, higher rotation rates were obtained using polarized Gaussian beams and birefringent particles. Trapped in a linearly polarized beam, a birefringent object was shown to align its optical axis along the direction of the electric field. Rotating the beam polarization leads to the rotation of the object itself.[8] In a related approach, using a circularly polarized Gaussian beam, trapped birefringent particles

1934-2608/2011/$25.00 © 2011 SPIE

were shown to rotate at rates exceeding 1 kHz.[9–12] More recently, it was shown that a linearly polarized Gaussian can be used to obtain more complex rotational dynamics of glass nanorods, namely, rotational oscillations of the rod around the optical axis.[13,14]

Microparticles were also rotated with optical tweezers that use asymmetric laser beams. For example, when an elongated object is trapped in a high order Hermite–Gaussian mode with an intensity distribution that consists of collinear spots it aligns along the trap axis. Moreover, rotating the beam around the optical axis rotates the trapped object accordingly.[15] Similarly, an elliptically shaped trap, obtained by inserting a rectangular aperture in the optical path of a Gaussian beam, was shown to rotate extended objects when the aperture is rotated.[16] A different approach uses a beam with a spiral intensity pattern to trap an aggregate consisting of three coplanar silica beads. While each bead is trapped in a different arm of the spiral, rotating the pattern around the axis of the beam rotates the entire aggregate.[17]

All the methods described above were designed to rotate particles around the optical axis, that is, in the image plane. However, the ability to view an object at different orientations plays an important role in the context of cellular imaging. For example, changing the angle between the optical axis and the long axis of a trapped cell, $\theta$, allows imaging three-dimensional (3D) sub-cellular structures from different viewpoints. Subsequently, such 3D structures can be reconstructed using methods similar to those developed for computerized tomography (CT). A technique that was previously used to rotate a trapped object around an arbitrary axis employs the scanning of a single optical Gaussian trap between multiple positions in the 3D space of the sample. It was shown that the object, effectively held by several traps, rotates whenever the positions of the traps move along appropriate trajectories.[18] Another approach uses a pair of adjacent LG traps, each holding a different part of the trapped object. Rotating the pair of traps around any desired axis rotates the object accordingly.[19]

In this article we present a new setup that allows rotating an elongated micro-object around an axis perpendicular to the optical axis.[20] A single optical trap is rapidly oscillated along a line normal to the optical axis, by means of a galvanometric mirror, to create a linear trap. Altering the oscillation amplitude, $A$, the length of the linear trap is varied between two extreme cases: 1. static trap ($A = 0$), where an elongated object is oriented along the optical axis (vertical orientation). 2. Long linear trap ($A > L/2$, where $L$ is the length of the trapped object), where the object is oriented along the trap axis (horizontal orientation). We demonstrate, using *E. coli* bacterial cells, that in the intermediate range, the alignment of the trapped object varies with the size of the trap between the vertical and the horizontal orientations covering the entire range of $\theta$. To monitor the rotation, we have developed a technique that allows finding the orientation of the cell from the corresponding phase contrast images.

## 2 Experimental Methods

### 2.1 Optical System

Our setup is based on an IX70 inverted Olympus microscope. The trapping is achieved using a diode laser (SDL, $\lambda = 830$ nm). Its power was set to 70 mW, corresponding to 37 mW at the exit from the objective lens (UPLFLN 100XO2PH, 1.3 NA, oil immersion). Before the beam enters the objective it is reflected from a single galvanometric mirror and expanded by the telescope lenses $L_1$ and $L_2$ (see Fig. 1). Lenses $L_1$ and $L_2$ also conjugate the plane of the galvanometric mirror to that of the objective back aperture. In this configuration, tilting the galvanometric mirror does not shift the beam as it enters the objective, but rather tilts it with respect to the optical axis (Fig. 1). Therefore, the truncation of the beam due to the objective is kept constant as the mirror rotates and the trap structure is preserved while it scans the image plane.[21] In our system, the beam is truncated at about $2.7\sigma$ of the Gaussian profile. Oscillating the galvanometric mirror via a function generator at low oscillation frequencies ($f < 30$ Hz) we find that the trapped cell moves along with the trap. Further increasing the frequency eventually leads to an effective linear trap. Its length is determined by the amplitude of the voltage function. In this regime the

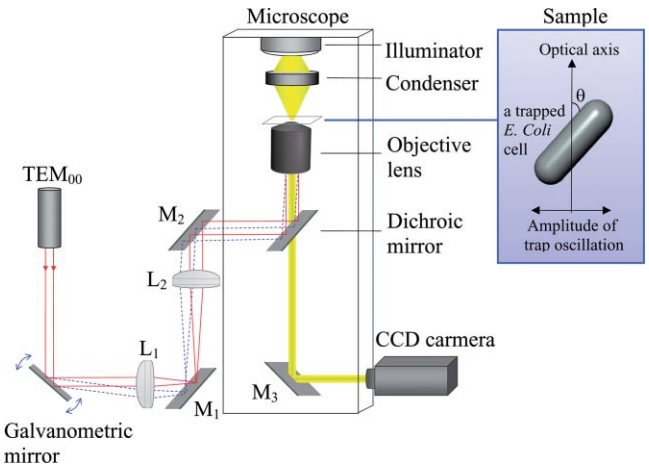


**Fig. 1** The optical system: $M_1$, $M_2$, and $M_3$—mirrors. $L_1$, $L_2$—telescope lenses that conjugate the planes of the galvanometric mirror and the objective back aperture. The laser beam is shown for the case when the galvanometric mirror is at 45 deg (full red line) and when it is rotated to a smaller angle (dashed blue line).

cell stops oscillating and aligns itself at an orientation determined by the oscillation amplitude. Although the exact transition frequency between the regimes was not determined, we find that at $f = 100$ Hz the system is sufficiently far from this transition in the linear trap regime. Moreover, no change in the trapping behavior was observed at higher frequencies. Therefore, all our cell rotation experiments were performed at $f = 100$ Hz. The position of the trap along the optical axis can be varied by slight changes in the distance between the telescope lenses $L_1$ and $L_2$. This determines the distance between the trapped object and the focal plane of the objective lens controlling the focusing degree of the image of a trapped object.

## 2.2 Rotating a Trapped E. coli Cell

Due to their elongated shape *E. coli* cells are suitable as test objects for our rotation method. In fact, their shape is almost exactly that of a cylinder with hemispherical caps[22] and their size is about $1 \times 3$ $\mu$m. Since *E. coli* have a highly rigid cell wall, their shape is not affected by the trapping forces.[23] The cells are grown in Lurie Broth medium until their optical density at 600 nm reaches 0.2, which is in the exponential growth regime. After growth, cells are fixed by adding 0.2% formaldehyde to the medium. The suspension of the cells is then diluted and placed in the microscope sample. The latter consists of two cover slips spaced with a parafilm ring. Moving the motorized microscope stage, a particular cell is brought to the vicinity of the trap. Due to the forces of the focused laser beam it becomes aligned along the optical axis [as shown in Fig. 2(a)]. Oscillating the trap along a line in the image plane changes the equilibrium orientation from $0^\circ$ to $\theta(A)$ leaving the cell in an unstable orientation. However, due to the symmetry of the trap, the opposite orientation, $-\theta(A)$, is also stable. It is the Brownian fluctuations ($5^\circ$ standard deviation for a vertically oriented cell in our setup) that determine whether the cell

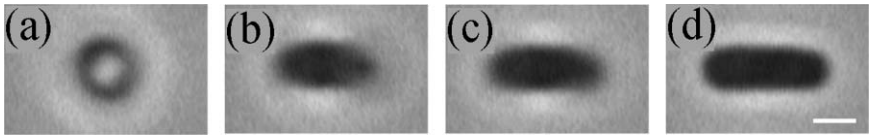


**Fig. 2** Phase contrast images of an *E. coli* cell trapped with optical tweezers. The cell rotates as the trap oscillation amplitude is increased from zero (a) to a value that slightly exceeds half of the cell length (d). Bar = 1 $\mu$m.

rotates clockwise [towards $\theta(A)$] or anticlockwise [towards $-\theta(A)$]. Alternatively, the choice of the stable orientation can be controlled using the flow of the liquid medium that occurs when the sample is moved. Since such flow tilts the cell, moving the sample at the onset of the trap oscillations allows choosing between the $\theta(A)$ and $-\theta(A)$ orientations. Therefore, in what follows, we refer to $\theta$ as a positive angle, $0 \text{ deg} < \theta < 90 \text{ deg}$, that grows with the oscillation amplitude [Figs. 2(b) and 2(c)]. When the trap length reaches the length of the cell, the latter becomes horizontally oriented [Fig. 2(d)]. All our results were obtained using a sinusoidal voltage wave to activate the galvanometric mirror. However, we found no observable difference in the rotation of the cell when other voltage wave forms were used, e.g., saw-tooth.

As was noted above, our main motivation for rotating a cell out of the image plane is the implementation of CT for a single bacterial cell. To this end, fluorescent images of stained 3D sub-cellular structures corresponding to different viewpoints need to be recorded. However, to reconstruct the 3D structures from these images, it is necessary to know the cell orientation angle $\theta$ for each such image.

Since phase contrast images contain information about the cell geometry, these are most appropriate for measuring $\theta$. However, the high magnification objective, which is essential for both trapping and acquiring detailed images of micron-sized objects, has a small depth of field relative to the dimensions of the trapped cell. Since in our system the depth of field is about 450 nm, the image of a 3-$\mu$m long cell appears focused only when the cell is oriented in the ($80^\circ$ to $90^\circ$) range of $\theta$. For all other cell orientations the image of the cell caps is smeared [see Figs. 2(b) and 2(c)] and locating the cell edge in order to measure $\theta$ is a challenging task. In Sec. 3, we present a technique using phase contrast images that include strongly defocused cell sections to measure the orientation of a trapped cell. This technique allows a controlled scan of the cell orientation over the entire $\theta$ range.

## 3 Results

### 3.1 Out of Focus Analysis

To find the orientation of a trapped cell we need to know both the cell dimensions and the length of its projection on the image plane. First, the cell dimensions are obtained using a horizontally oriented cell image. We use an edge detection method, developed in Ref. 24, to find the contour of the cell with high accuracy. From this contour we then compute the radius and length of the cell. Next, we need to locate the cell end points in the rotated cell image to find the length of the cell projection on the image plane. Since the cell ends are defocused in those images, we study the behavior of the cell image as a function of the defocusing level.

In the first stage of the defocus analysis, the trapped cell is oriented horizontally, $\theta = 90^\circ$. Then the height of the trap relative to the focal plane is varied by means of small, stepwise changes in the distance between the telescope lenses, $L_1$ and $L_2$. Consequently, the cell image corresponds to a different defocusing level at each such step (see Fig. 3). In what follows, we refer to the set of images resulting from this procedure as the height library.

Next, we plot the longitudinal intensity profiles of the height library images (see Fig. 4). These profiles represent the intensity values of the images along the long axis of the cell. To reduce the noise level, the intensities are averaged over 10 consecutive frames recorded at each step of the height scan. Although the intensity profiles are quite different from each other we find that they intersect, within experimental error, at two locations (Fig. 4). We refer to these locations as critical points. This behavior is reminiscent of the focus invariant intensity points in the bright field image of a semitransparent straight edge.[25,26] It is worthwhile to note that, for a given distance from the focal plane, trapped cell images above and below the focal plane can be rather different. Nevertheless, we find that the intersection of the longitudinal intensity profiles occurs at the same points on both sides of the focal plane.

Comparing the locations of the critical points with those of the cell ends that are extracted from the focused image of the height library,[24] we find that the critical points are located 135

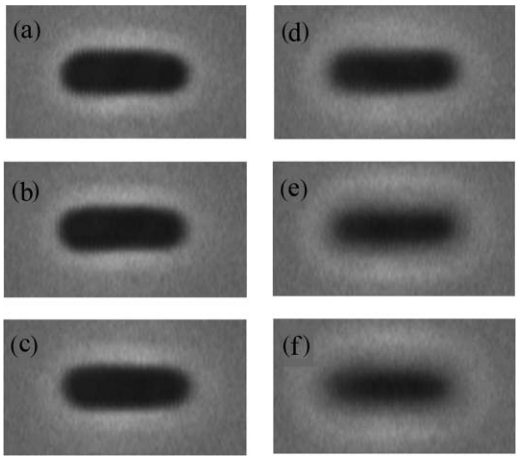


**Fig. 3** The height library for the same cell as in Fig. 2. The trap is scanned from the focal plane (a) toward its most defocused position at about 1.5 $\mu$m above the focal plane (f).

$\pm$ 36 nm (average over 29 cells $\pm$ standard deviation) outside the cell. Therefore, the distance between the critical points positions, $L_{\mathrm{cp}}$, is on average larger by about 10% than the cell length, $L$, providing an approximation to the cell length. The intersection of all the intensity profiles at the critical point indicates that within a few micrometers of the focal plane, $L_{\mathrm{cp}}$ is invariant under defocusing translations and so is the value of the phase contrast intensity at the critical points, $I_{\mathrm{cp}}$. Assuming that $I_{\mathrm{cp}}$ is not affected by rotation, each of the defocused cell caps will have its own critical point in the rotated cell image, located where its longitudinal intensity profile equals $I_{\mathrm{cp}}$. As in the horizontal orientation, these critical points lie in the vicinity of the cell edge. It follows that the distance between the critical points of the rotated cell corresponds to the projected $L_{\mathrm{cp}}$ on the imaging plane, $L_{cp}\sin\theta$, allowing to deduce $\theta$. The critical point approach fails at angles that are less than about 25° where, in the image, the cylindrical section of the cell largely overlaps with its caps (see Fig. 7).

The critical point method described above allows measuring the orientation of a rotated cell. However, the validity of the assumption that $I_{\mathrm{cp}}$ is invariant under cell rotations, on which the method relies, remains to be verified. To this end, we compared the results of the critical point method with those obtained from a second, independent method. The key of this comparison is that both methods are applied to the same cell with a fixed orientation. In Sec. 3.2, we present a detailed description of this procedure employing cells attached to the glass bottom of the sample.

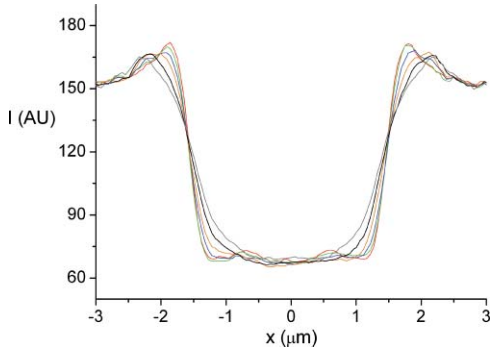


**Fig. 4** Longitudinal intensity profiles of the height library images shown in Fig. 3.

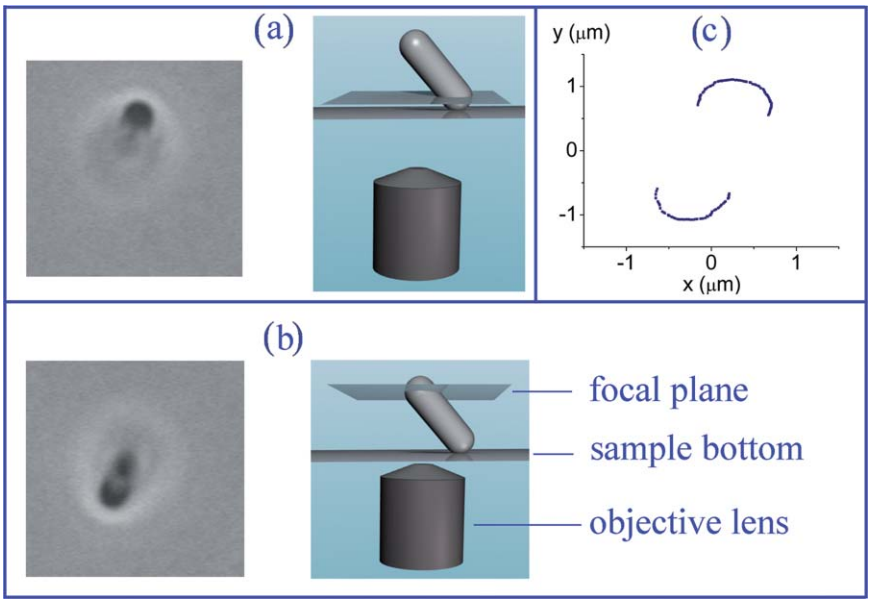


**Fig. 5** Imaging the caps of the same cell as in Figs. 2,3, and 4 while it is immobilized on the glass bottom of the sample. (a) The focus is on the lower cell cap. (b) The focus is on the higher cell cap. (c) Each of the images in (a) and (b) are analyzed to obtain the contours of the caps. The overlay of the two cap contours is used to find the length of the cell projection on the image plane. We obtain that the orientation angle of this cell is 49 deg.

### *3.2 Measuring the Orientation of Immobilized Cells*

In PBS buffer with $p\mathrm{H} = 7.4$ *E. coli* cells display a large affinity to glass surfaces. Thus, upon contact with a glass surface, cells become irreversibly attached to it and their Brownian motion is reduced below the resolution of our system (about 40 nm). Using our ability to orient a trapped cell, we can lower cells toward the glass bottom of the sample while holding them inclined relative to the optical axis. We find that when the cell attaches to the glass it preserves this inclination allowing to control the value of $\theta$ for the immobilized cells.

The steps of our procedure are as follows. Once the cell is trapped, a height library is recorded to obtain the values of the corresponding $I_{\mathrm{cp}}$ and $L_{\mathrm{cp}}$. Then, we set the oscillation amplitude of the trap to obtain the desired cell orientation. To bring the cell into contact with the glass bottom we raise the microscope stage while keeping the trap in place. Following cell immobilization, the trap is turned off. Next, we move the objective to obtain a focused image of each of the cell caps separately, as shown in Figs. 5(a) and 5(b). Applying the edge detection method described in Ref. 24 on each of the cap images, we find the contour of the corresponding edge [see Fig. 5(c)]. The maximal distance between two points, each belonging to another cap, represents the projection length of the cell on the image plane. Using our procedure, it is measured with an accuracy of 40 nm. For small $\theta$'s, $\theta < 25^{\circ}$, we cannot find the contour of the caps due to their overlap with the cylindrical part (see Fig. 7). Hence, this method only holds for $\theta$'s larger than $25^{\circ}$. The cell length and radius are extracted from the contour of the focused frame in the height library. A simple geometric relation between the cell length, radius, and projection length allows finding the orientation angle. Accordingly, we refer to this procedure as the geometric method and the resulting angle as $\theta_{\mathrm{g}}$.

The immobilized cell that was analyzed following the procedure of the previous paragraph can also be imaged focusing on the center of the cell. Such image is equivalent to the one obtained for an obliquely oriented trapped cell where both its caps appear defocused. Using the height library, such image can be analyzed applying the critical point method to obtain the orientation angle. We denote this angle as $\theta_{\mathrm{cp}}$.

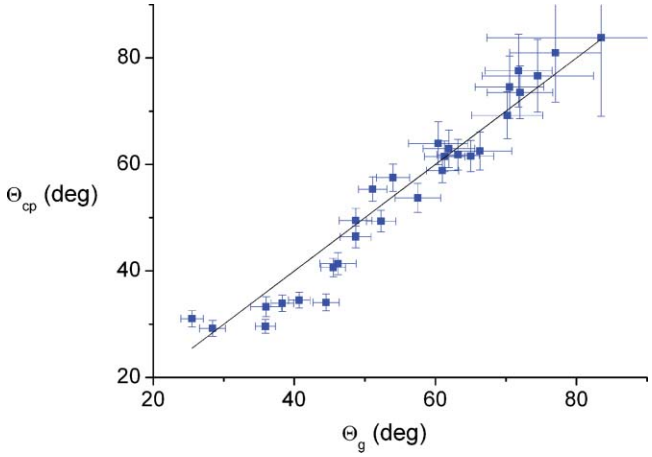


**Fig. 6** Testing the critical point method. For *E. coli* cells that were attached to the glass bottom of the sample in different orientations we compare $\theta_{cp}$ with $\theta_g$ (blue squares). The $\theta_{cp} = \theta_g$ line is also shown.

The experiment described above, where both the critical point and the geometric methods are applied on the same cell, was performed for 29 different cells that each was attached to the glass with a different orientation. In Fig. 6 we show the comparison between the results of the two methods. Note the good agreement between the values of $\theta_{cp}$ and $\theta_g$. The deviations of the data from the $\theta_{cp} = \theta_g$ line at angles below $50^\circ$ could be due to cell shapes that slightly differ from a perfect cylinder with hemispherical caps.

### *3.3 Scanning the Orientation of a Trapped Bacterial Cell*

Using the critical point method, we can monitor the rotation of a trapped cell as long as the orientation angle, $\theta$, lies between 25 and $90^\circ$. To estimate the value of $\theta$ in the (0 to $25^\circ$) range we approximate the cell image with that of a slightly inclined cylinder. Since the depth of field of our microscope is significantly smaller than the cell length, $L$, we expect that the image of a slightly inclined cylinder displays intensity contours parallel to the section of the cylinder. The shape of such section is elliptical and the ratio between its long and short axes, $R_{LS}(\theta)$, grows with increasing $\theta$, $R_{LS}(\theta) = 1/\cos\theta$. Indeed, in the small $\theta$ range, the intensity contours of the cell image are approximately elliptical (see Fig. 7). We use the contour which corresponds to an intensity slightly below the background level to determine $R_{LS}(\theta)$ and hence $\theta$. Since the geometrical method of the Sec. 3.2 fails in the range of small $\theta$'s we could not test the accuracy of the orientation obtained using this approach. In Fig. 7 we show a $\theta$-scan with a $10^\circ$ step for

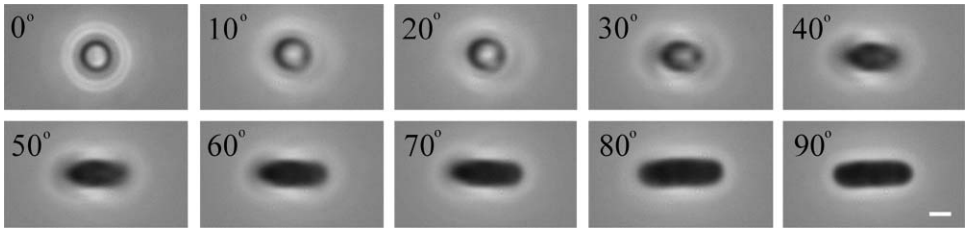


**Fig. 7** A $\theta$-scan of an *E. coli* cell. Angles between 30 and 90 deg were measured using the critical point method, 10 deg and 20 deg are obtained using the elliptical approximation to the intensity contour (see text) and 0 deg corresponds to the case of the nonoscillating trap. Bar $= 1\ \mu$m.

a typical *E. coli* cell. It is obtained by varying the trap oscillation amplitude, $A$, from 0 to $L/2$, corresponding to the entire range of $\theta$.

## 4 Discussion

In this article we presented an optical tweezers setup that allows rotating elongated objects around an axis normal to the optical axis. Our setup requires the inclusion of an oscillating mirror along the optical path of a standard optical tweezers system to create a linear trap. This setup is significantly simpler then that of the alternative techniques.[18,19] Moreover, unlike the other techniques, our approach does not use several traps that hold the object at different points. Since there is a limit on the minimal possible distance between two optical traps, multiple trap methods are restricted to rotating relatively large objects. The smallest object rotated relative to the optical axis using multiple traps was a fused pair of 2-$\mu$m diameter beads. This was done employing LG traps that are narrower along the optical axis than Gaussian traps.[19] Our technique can rotate a bacterial cell of about the same size as the fused beads without the need of higher order beams.

To further control the rotation we introduced an edge detection method for defocused images. It was utilized to find the orientation of rotated cells and allowed monitoring the rotation of cells over the entire orientation range.

We suggest that our controlled alignment technique may become a useful tool in cellular imaging, since it can provide different viewpoints on 3D sub-cellular structures. In particular, it could be used for the realization of CT imaging of a bacterial cell. We should first calibrate the relation between the orientation angle and the trap oscillation amplitude, $\theta(A)$, using the critical point method together with phase-contrast imaging. Such calibration will allow performing an equal step $\theta$-scan of the same cell while fluorescently imaging one of its 3D structures, e.g., the nucleoid.

Our setup can be further upgraded. Adding a second scanning axis for the laser beam in the image plane, the linear trap can also be rotated around the optical axis. This would allow controlling the orientation of an elongated object with respect to two normal axes. Together with the 3D translation of the motorized microscope stage, it enables control over 5 deg of freedom for a trapped elongated object using a single linear trap. This setup could be applied for optical microassembly where microfabricated building blocks are maneuvered to build complex structures.[27]

## Acknowledgments

We thank I. Abdulhalim, A. Braiman, and I. Fishov for useful discussions. This research was supported in part by the Israel Academy of Science and Humanities (Grant No. 1544/08).

## References

1. A. Ashkin, J. M. Dziedzic, J. E. Bjorkholm, and S. Chu, "Observation of a single-beam gradient force optical trap for dielectric particles," *Opt. Lett.* **11**, 288–290 (1986).
2. A. Ashkin, J. M. Dziedzic, and T. Yamane, "Optical trapping and manipulation of single cells using infrared laser beams," *Nature (London)* **330**, 769–771 (1987).
3. H. Misawa, K. Sasaki, M. Koshioka, N. Kitamura, and H. Masuhara, "Multibeam laser manipulation and fixation of microparticles," *Appl. Phys. Lett.* **60**, 310–312 (1992).
4. E. Higurashi, H. Ukita, H. Tanaka, and O. Ohguchi, "Optically induced rotation of anisotropic micro-objects fabricated by surface micromachining," *Appl. Phys. Lett.* **64**, 2209–2210 (1994).
5. H. He, M. E. J. Friese, N. R. Heckenberg, and H. Rubinsztein-Dunlop, "Direct observation of transfer of angular momentum to absorptive particles from a laser beam with a phase singularity," *Phys. Rev. Lett.* **75**, 826–829 (1995).

6. M. E. J. Friese, J. Enger, H. Rubinsztein-Dunlop, and N. R. Heckenberg, "Optical angular-momentum transfer to trapped absorbing particles," *Phys. Rev. A* **54**, 1593–1596 (1996).
7. N. B. Simpson, K. Dholakia, L. Allen, and M. J. Padgett, "Mechanical equivalence of spin and orbital angular momentum of light: an optical spanner," *Opt. Lett.* **22**, 52–54 (1997).
8. E. Higurashi, R. Sawada, and T. Ito, "Optically induced angular alignment of birefringent micro-objects by linear polarization," *Appl. Phys. Lett.* **73**, 3034–3036 (1998).
9. M. E. J. Friese, T. A. Neiminen, N. R. Heckenberg, and H. Rubinsztein-Dunlop, "Optical alignment and spinning of laser-trapped microscopic particles," *Nature* **394**, 348–350 (1998).
10. S. Juodkazis, M. Shikata, T. Takahashi, S. Matsuo, and H. Misawa, "Fast optical switching by a laser-manipulated microdroplet of liquid crystal," *Appl. Phys. Lett.* **74**, 3627–3629 (1999).
11. E. Higurashi, R. Sawada, and T. Ito, "Optically induced angular alignment of trapped birefringent micro-objects by linearly polarized light," *Phys. Rev. E* **59**, 3676–3681 (1999).
12. E. Higurashi, R. Sawada, and T. Ito, "Optically driven angular alignment of microcomponents made of in-plane birefringent polyimide film based on optical angular momentum transfer," *J. Micromech. Microeng.* **11**, 140–145 (2001).
13. K. Bonin, B. Kourmanov, and T. Walker, "Light torque nanocontrol, nanomotors and nanorockers," *Opt. Express* **10**, 984–989 (2002).
14. W. A. Shelton, K. D. Bonin, and T. G. Walker, "Nonlinear motion of optically torqued nanorods," *Phys. Rev. E* **71**, 036204 (2005).
15. S. Sato, M. Ishigure, and H. Inaba, "Optical trapping and rotational manipulation of microscopic particles and biological cells using higher-order mode Nd:YAG laser beams," *Electron. Lett.* **27**, 1831–1832 (1991).
16. A. T. O'Neil and M. J. Padgett, "Rotational control within optical tweezers by use of a rotating aperture," *Opt. Lett.* **27**, 743–745 (2002).
17. L. Paterson, M. P. MacDonald, J. Arlt, W. Sibbett, P. E. Bryant, and K. Dholakia, "Controlled rotation of optically trapped microscopic particles," *Science* **292**, 912–914 (2001).
18. K. Visscher, G. J. Brakenhoff, and J. J. Krol, "Micromanipulation by "multiple" optical traps created by a single fast scanning trap integrated with the Bilateral Confocal Scanning Laser Microscope," *Cytometry* **14**, 105–114 (1993).
19. V. Bingelyte, J. Leach, J. Courtial, and M. J. Padgett, "Optically controlled three-dimensional rotation of microscopic objects," *Appl. Phys. Lett.* **82**, 829–831 (2003).
20. G. Carmon and M. Feingold, "Rotation of single bacterial cells relative to the optical axis using Optical Tweezers," *Opt. Lett.* **36**, 40–42 (2011).
21. E. Fällman and O. Axner, "Design for fully steerable dual-trap optical tweezers", *Appl. Opt.* **36**, 2107–2113 (1997).
22. E. Itan, G. Carmon, A. Rabinovitch, I. Fishov, and M. Feingold, "The shape of non-septated *E. coli* is asymmetric," *Phys. Rev. E* **77**, 061902 (2008).
23. X. Yao, M. Jericho, D. Pink, and T. Beveridge, "Thickness and elasticity of Gram-negative murein sacculi measured by atomic force microscopy," *J. Bacteriol.* **181**, 6865–6875 (1999).
24. G. Reshes, S. Vanounou, I. Fishov, and M. Feingold, "Cell shape dynamics in *E. coli*," *Biophys. J.* **94**, 251–264 (2008).
25. A. Glindemann and J. Kross, "Symmetry in partially coherent imaging of semi-transparent edges," *J. Mod. Opt.* **38**, 379–394 (1991).
26. M. Gu and C. J. R. Sheppard, "Effects of defocus and primary spherical aberration on images of a straight edge in confocal microscopy," *Appl. Opt.* **33**, 625–630 (1994).
27. P. J. Rodrigo, L. Kelemen, D. Palima, C. A. Alonzo, P. Ormos, and J. Glückstad, "Optical microassembly platform for constructing reconfigurable microenvironments for biomedical studies," *Opt. Express* **17**, 6578–6583 (2009).


Biographies and photographs of the authors not available.